Nanoscale

A Unique 19F MRI Agent for the Tracking of Non Phagocytic Cells In Vivo

Journal:	*Nanoscale*
Manuscript ID	NR-ART-01-2018-000703.R2
Article Type:	Paper
Date Submitted by the Author:	09-Apr-2018
Complete List of Authors:	Moonshi, Shehzahdi; University of Queensland, AIBN Zhang, Cheng; The University of Queensland, Australian Institute for Bioengineering and Nanotechnology Peng, Hui; University of Queensland, Australian Institute for Bioengineering and Nanotechnology Puttick, Simon; University of Queensland, AIBN; ARC Centre of Excellence in Convergent BioNano Science, Rose, Stephen; CSIRO, The Australian e-Health Research Centre Fisk, Nicholas; University of New South Wales Bhakoo, Kishore; Singapore Bioimaging Consortium (SBIC), A*STAR, Stringer, Brett; QIMR Berghofer Medical Research Institute, Qiao, Greg; The University of Melbourne, Chemical and Biomolecular Engineering Gurr, Paul; The University of Melbourne, Chemical and Biomolecular Engineering Whittaker, Andrew; University of Queensland, Australian Institute for Bioengineering and Nanotechnology

A Unique ^{19}F MRI Agent for the Tracking of Non Phagocytic Cells *In Vivo*

Shehzahdi S. Moonshi[a‡], Cheng Zhang[a‡], Hui Peng,[a] Simon Puttick[a], Stephen Rose[b], Nicholas M. Fisk[c], Kishore Bhakoo[d], Brett W. Stringer[e], Greg G. Qiao[f], Paul A. Gurr[g] and Andrew K. Whittaker*[a]

[a]Australian Institute for Bioengineering and Nanotechnology and ARC Centre of Excellence in Convergent Bio-Nano Science and Technology, The University of Queensland, QLD 4072, Australia. Email: a.whittaker@uq.edu.au

[b]UQ Health Science Building, Royal Brisbane and Women's Hospital, QLD 4029, Australia

[c]UQ Centre for Clinical Research, The University of Queensland, QLD 4029, Australia

[d]Singapore Bioimaging Consortium (A*STAR), Helios 138667, Singapore

[e]QIMR Berghofer Medical Research Institute, QLD 4006, Australia

[f]Department of Chemical and Biomolecular Engineering, Cooperative Research Centre for Greenhouse Gas Technologies, The University of Melbourne, Victoria 3010, Australia

[g]Department of Chemical and Biomolecular Engineering, The University of Melbourne, Victoria 3010, Australia

Keywords: ^{19}F MRI, dual-modal agent, cell tracking, mesenchymal stem cells

ABSTRACT

There is currently intense interest in new methods for understanding the fate of therapeutically-relevant cells, such as mesenchymal stem cells (MSCs). The absence of a confounding background signal and consequent unequivocal assignment makes ^{19}F MRI one of the most attractive modalities for the tracking of injected cells in vivo. We describe here the synthesis of novel partly-fluorinated polymeric nanoparticles with small size and high fluorine content as MRI agents. The polymers, constructed from perfluoropolyether methacrylate (PFPEMA) and oligo(ethylene glycol) methacrylate (OEGMA) have favourable cell uptake profiles and excellent MRI performance. To facilitate cell studies the polymer was further conjugated with a fluorescent dye creating a dual-modal imaging agent. The efficacy of labelling of MSCs was assessed using ^{19}F NMR, flow cytometry and confocal microscopy. The labelling efficiency of $2.6 \pm 0.1 \times 10^{12}$ ^{19}F atoms per cell, and viability of >90 % demonstrates high uptake and good tolerance by the cells. This loading translates to a minimum ^{19}F MRI detection sensitivity of ~ 7.4×10^3 cells/voxel. Importantly, preliminary *in vivo* data demonstrate that labelled cells can be readily detected within a short acquisition scan period (12 minutes). Hence, these copolymers show outstanding potential for ^{19}F MRI cellular tracking and for quantification of non-phagocytic and therapeutically-relevant cells *in vivo*.

1. INTRODUCTION

Mesenchymal stem/stromal cells (MSCs), a type of adult stem cell, have recently attracted enormous interest for the treatment of a broad range of diseases, with almost 600 clinical trials involving MSCs listed in the clinical trials database (http://clinicaltrials.gov/).[1] In these studies, MSCs have been exploited either as therapeutic agents or as delivery systems.[2] The broad utility of MSCs is now recognized as being due to a range of properties in addition to their capacity for differentiation,[3] including immunomodulation and immunosuppression,[4] inherent tropism to injured tissue/tumor microenvironments [5] and inhibitory effects on several tumor types.[6] Despite this promise, translation of MSC-based therapies to the clinic remains challenging and results have often been discouraging.[7] The full therapeutic potential of MSCs can only be attained if they migrate and home to the sites of lesion, survive and engraft post implantation. The lack of tools to understand the fate of transplanted cells, non-invasively and longitudinally, is in part responsible for conflicting clinical trial results.[8] Unfortunately, conventional imaging modalities for the tracking stem cells in the laboratory such as fluorescence and bioluminescence imaging have limited potential for clinical translation.[1, 9]

In vivo cell tracking is potentially a powerful tool to monitor non-invasively the distribution and accumulation of therapeutic cells such as MSCs. Development of accurate imaging modalities to track MSCs would allow clinicians to determine whether cell delivery has occurred at the appropriate site and if cells remain at their targeted location.[10] Consequently, non-invasive real-time imaging techniques need to be developed to ascertain homing efficiency, dosing requirements, optimal timing and route of delivery to allow success of cell-based therapies.[10]

In recent years an array of imaging modalities including magnetic resonance imaging (MRI), positron emission tomography (PET), computed tomography (CT), single-photon emission computed tomography (SPECT), ultrasound (US), fluorescence and bioluminescence imaging (BLI) have become available for *in vivo* cell tracking, with each technique having advantages and

limitations.[11] MRI is a particularly promising imaging modality for serial tracking of MSCs[12] as it does not involve the use of ionizing radiation and is appropriate for deep tissue imaging at high resolution.[11] Tracking is achieved by pre-labelling MSCs prior to implantation with an imaging agent (molecular or particulate) which provides a change in image intensity on an MRI scan.[13] The MRI signal can be generated and moderated in several ways including with positive contrast agents containing paramagnetic metals (e.g. gadolinium), negative contrast agents comprised of superparamagnetic iron oxides (SPIO) or partly-fluorinated molecules or particles for ^{19}F MRI.[14]

In the early 1990's Weissleder *et al.* observed that SPIOs and ultra-small superparamagnetic iron oxides (USPIOs) accumulate in endosomes following endocytosis, resulting in an amplification of their susceptibility effects and hence efficacy as MRI contrast agents.[15] Since then, T_2/T_2* contrast agents have been the most broadly utilized agents for tracking of stem cells using MRI.[16] A number of preclinical *in vivo* studies tracking MSCs using SPIOs has been reported in various animal models.[17, 18] However, the approach of labelling cells with superparamagnetic iron oxide particles for cell tracking has limitations. While single cells can be distinguished *in vivo* under certain conditions,[19] the negative contrast produced by SPIO-labelled cells can be confounded by other low signal media such as blood, bone and air.[20] Therefore, it is often challenging to unequivocally identify regions containing labelled cells in settings of traumatic injury with haemorrhage.[21] Moreover, quantification of iron-labelled cells is difficult as a consequence of susceptibility artefacts. Indirect quantification of labelled cells involves the measure of "signal void volume" or the "number of black pixels" and is determined by the change in image intensity relative to the image before injection.[22] Contrast generated by SPIO-labelled cells is attained indirectly through observation of changes in relaxation properties of surrounding water molecules; all of these factors make quantification of the number of labelled cells *in vivo* highly challenging.[12]

An alternative approach to cell quantification is through ^{19}F MRI, where cells are labelled with fluorinated molecules or nanoparticles.[12] ^{19}F MRI provides high contrast-to-noise ratio and excellent specificity due to the absence of a background signal. Therefore, the signal obtained is

specific to labelled cells unlike metal ion-based cell labelling methodologies where false positive cell detection is possible.[23] The ^{19}F nucleus has 100% natural abundance, and is appropriate for labelling as its MR sensitivity is just 17% less than that of ^{1}H[13] and the ^{19}F NMR resonance frequency is 94% of that of ^{1}H.[23] However, the technique is potentially less sensitive in comparison to labelling and tracking with metal-based agents for the detection of small cell numbers (e.g. single cell detection has been demonstrated).[11] Although the signal-to-noise ratio (SNR) of the ^{19}F MR images may be lower in comparison to ^{1}H MRI, a high ^{19}F MRI SNR is not required since this atom is largely absent from the body, and when present cannot be detected by conventional MRI methods.[10] Thus the apparent disadvantage of lower sensitivity is compensated for by the lack of background signal in ^{19}F MR images allowing cell detection to be unequivocal.[14]

^{19}F MRI does not however provide anatomical information and hence ^{19}F MR images are overlaid on a ^{1}H MRI anatomical image acquired concurrently with the same scanner, in order to avoid image misregistration.[24] As indicated above, ^{19}F MRI allows for quantification of injected cells as the signal intensity is, in principle, directly proportional to the number of ^{19}F nuclei present. Therefore, the *in vivo* image can provide a quantitative measure of cell numbers when the average content of ^{19}F spins per cell is known.[25] Consequently, ^{19}F MRI provides a highly specific, unambiguous and quantitative approach of tracking of labelled MSCs.

Recently, intense effort has been committed to the development of ^{19}F MRI agents, including perfluorocarbon (PFC) emulsions, ^{19}F-containing small molecules and ^{19}F-containing macromolecules.[26-41] The richness of the chemistry of fluorinated organic compounds from small molecules to macromolecules provides tremendous possibilities for the development of ^{19}F MRI agents. PFCs are some of the most common trackers used in ^{19}F imaging. Moreover, PFCs have distinctive characteristics such as high hydrophobicity, significant lipophobicity, extremely low intermolecular cohesion, low surface tension and high biological stability.[10]

In recent years, particles containing perfluoropolyethers (PFPE) have been presented as attractive ^{19}F imaging agents due to their simple ^{19}F NMR spectrum and relative ease of synthesis.[42,

[43] PFPEs, in particular linear perfluorinated polymers, are not soluble in water and require incorporation with hydrophilic segments or within an emulsion. The majority of ^{19}F MRI cell labelling studies reported have employed the commercial product Celsense, which are PFC emulsions (typical sizes from 100 to 300 nm) based on linear PFPE polymer mixtures.[12, 44] Several studies have demonstrated MR detection of ^{19}F labelled stem cells *in vivo,* and four studies have reported longitudinal imaging of the fate of these cells post transplantation.[12, 21, 45, 46] These studies involved labelling of neural stem cells (NSCs) with PFC nanoemulsions, apart from a single report which utilized labelled bone marrow derived MSCs in a healthy mouse model. However, a concern with nanoemulsions is the inevitable process of Ostwald ripening which results in growth of larger particles at the detriment of the smaller particles.[47] Additionally, the chemical inertness of nanoemulsions limits their potential application due to a lack of available sites for chemical modification. Finally, the large size of nanoemulsions can cause the agents to be retained within the organs of the animal for an extended period of time.[10]

In order to address these drawbacks, partially-fluorinated polymers (PFPs) have been proposed as alternative ^{19}F MRI agents.[26] Fluorine-containing polymers are readily prepared for example via copolymerization of fluorinated monomers with hydrophilic monomers. A large range of structures of PFPs can be envisaged, allowing attachment of various functional groups which provide a combination of different imaging modalities, therapeutic agents and targeting moieties for more specific and directed imaging in the body.[48] Furthermore, PFPs are highly stable and their generally smaller sizes lead to shorter, but controllable retention times in the body. Several groups have introduced unique PFPs as ^{19}F MRI CAs via combination of fluorinated monomers with hydrophilic or functional segments through chemical polymerizations.[26] In a study from our group, Thurecht *et al.* described the preparation of hyperbranched polymers (HBPs) with a fluorine content of ~ 2.5 wt. %, with 2,2,2-trifluoroethyl acrylate (TFEA) as the fluorine monomer, ethylene glycol dimethacrylate (EGDMA) as the crosslinking monomer and oligo(ethylene glycol) methyl ether methacrylate (OEGMA) as the hydrophilic monomer. These HBP molecules have been imaged

successfully in a mouse model following systemic injection, in a scan period of less than 10 minutes.[27] However, despite considerable advances, the use of PFPs as MRI contrast agents is often limited by low fluorine content (often below 5 wt. %) leading to low imaging sensitivity. The monomers 2,2,2-trifluoroethyl acrylate (TFEA) or 2,2,2-trifluoroethyl methacrylate (TFEMA) are commonly used as the fluorine-containing monomer for the synthesis of PFP contrast agents, but these monomers possess a relatively low weight-fraction of fluorine. Therefore, to achieve higher imaging sensitivity, novel monomers with a higher fluorine content should be investigated.

Here we describe the design and synthesis of novel fluorinated copolymers using a novel perfluoropolyether methacrylate (PFPEMA) as the fluorinated monomer and oligo(ethylene glycol) methacrylate (OEGMA) as the hydrophilic component necessary to impart solubility in aqueous media. The poly(OEGMA-*co*-PFPEMA) was modified by conjugation with a fluorescent dye to allow parallel validation studies (flow cytometry and microscopy), creating a dual-modal imaging agent. The polymers were characterized by ^{1}H, ^{19}F NMR, size exclusion chromatography (SEC) and dynamic light scattering (DLS) and loaded into human MSCs derived from term placenta (PMSCs) as they are abundant, involve non-invasive donor procurement, do not elicit ethical concerns and hence, are a therapeutically-relevant source of MSCs.[49, 50] The efficacy of labelling of the PMSCs was assessed using ^{19}F NMR and corroborated with flow cytometry and confocal fluorescence microscopy. *In vitro* and *in vivo* ^{19}F MR imaging of labelled PMSCs were conducted at a field strength of 9.4 T and showed high sensitivity allowing the acquisition of high resolution images in short acquisition times. Importantly, we confirmed that these copolymers did not alter the phenotypical and tri-lineage differentiation potential of MSCs. Our results suggest that this dual-modal ^{19}F MRI probe is a particularly promising nanoparticle system for tracking and quantification of non-phagocytic and therapeutically-relevant cells such as MSCs.

2. EXPERIMENTAL METHODS

2.1 Materials

All chemicals were reagent grade and utilized without further purification unless specified. Oligo(ethylene glycol) methyl ether methacrylate (OEGMA, MW = 475 g mol^{-1}) was purchased from Sigma-Aldrich and passed through basic alumina columns to remove inhibitors prior to use. Monohydroxy-perfluoropolyether (PFPE-OH, ~1650 g mol^{-1}) was supplied by Apollo Scientific Ltd, UK. The RAFT agent, 4-cyanopentanoic acid dithiobenzoate (CPADB), was synthesized according to a previously-reported method.[51] Deuterated solvents ($CDCl_3$ and D_2O) were purchased from Cambridge Isotope Laboratories.

Dulbecco's modified Eagle medium (DMEM) with high glucose, phosphate-buffered saline (PBS), Tryple Express, fetal bovine serum (FBS), antibiotic-antimycotic (AA), ActinRed™ 555 reagent, StemPro Differentiation kits , CellTrace™ CFSE Cell Proliferation Kit and membranes for dialysis (molecular weight cut-off of 3500 Da) were purchased from ThermoFisher Scientific. Gelatin was obtained from VWR Chemicals. Paraformaldehyde (PFA), trifluoroacetic acid (TFA), methacryloyl chloride, α,α,α-trifluorotoluene (TFT), *N*-(5-fluoresceinyl) maleimide, *n*-hexyl amine, dimethylphenyl phosphine (DMPP), cell counting kit-8 (CCK-8) were obtained from Sigma Aldrich. Mounting media with DAPI was purchased from Vector Laboratories.

2.2 Characterization of copolymer

^{1}H NMR, ^{19}F NMR and ^{19}F T_1 and T_2 relaxation times of the poly(OEGMA-*co*-PFPEMA) copolymers were measured at 9.4 T using a Bruker Avance III 400 MHz spectrometer fitted with a broadband BBFO probe with ^{19}F acquisition on the X channel. Cells in three T175 flasks were cultured in a solution containing the poly(OEGMA-*co*-PFPEMA) at a concentration of 20 mg mL^{-1} for 24 h and then fixed with 4 % paraformaldehyde (PFA) for 30 min. The samples were transferred into 3 mm NMR tubes and inserted into 5 mm NMR tubes filled with D_2O. The volume of the cells

was sufficient to fill the detector region of the NMR coil, typically ~ 4 cm in length from the bottom of the NMR tube. Acquisition of ^{19}F NMR spectra and measurements of T_1 and T_2 relaxation times were carried out at 310 K. ^{19}F NMR spectra of labelled cells were obtained using a relaxation delay of 1 s, acquisition time of 1.26 s and the number of scans was 1024. The ^{19}F spin-spin (T_2) relaxation times were measured using the Carr-Purcell-Meiboom-Gill (CPMG) pulse sequence at 310 K. The relaxation delay was 1 s, the acquisition time was 0.16 s and 64 scans were acquired. For each measurement, the echo times were varied from 2 to 770 ms and 16 points were collected. ^{19}F spin-lattice (T_1) relaxation times were measured using the standard inversion-recovery pulse sequence. The relaxation delay was 2 s, the acquisition time was 0.16 s and the number of scans was 32. For each measurement, the recovery times were varied from 2 ms to 3 s and 16 points were collected.

DLS measurements were acquired using a Nanoseries Zetasizer (Malvern, UK) with a 2 mW He-Ne laser functioning at wavelength of 633 nm and a scattering angle of 173°. Hydrodynamic diameter was measured twice to obtain an average value. The concentration of the copolymer was 1 mg mL^{-1}. SEC was performed on a Waters Alliance 2690 separations module equipped with an RI detector. The polymer was dissolved in tetrahydrofuran (THF), passed through 0.45 μm filter, and eluted at 1 mg mL^{-1} in THF.

2.3 Synthesis of perfluoropolyether methacrylate and poly(OEGMA-co-PFPEMA)

Into a two-neck flask fitted with a dropping funnel, stirrer bar and purged with N_2, monohydroxy-terminated perfluoropolyether (PFPE-ol) (1.65 kDa, 2.0 g, 1.21 mmol), triethylamine (211 μL, 0.153 g, 1.52 mmol), 2,6-di-t-butyl-4-methylphenol (20 mg) in α,α,α-trifluorotoluene (2 mL) (TFT) were added. Methacryloyl chloride (142 μL, 0.152 g, 1.45 mmol) was added dropwise at 0 °C, stirred for 1 h at this temperature, and then allowed to warm to room temperature overnight. The mixture was then diluted with TFT (20 mL), poured into water (50 mL) and the organic phase was washed with HCl (5%, 2 x 50 mL), NaOH (2 x 50 mL) and water to neutrality followed by drying over $MgSO_4$. The product was collected by filtration through a sintered glass funnel, before

being reduced to dryness under vacuum (0.1 mmHg). The perfluoropolyether methacrylate (PFPEMA), a colorless oil, was treated with another portion of 2,6-di-t-butyl-4-methylphenol (20 mg), sealed under N_2 and stored below 5 °C.

The copolymerization of OEGMA and PFPEMA was conducted as follows. In a typical experiment, OEGMA (1.2 g, 5 mmol), PFPEMA (1.73 g, 1 mmol), V40 (4.89 mg, 0.02 mmol), and CPADB (27.9 mg, 0.1 mmol) were dissolved in 5 mL TFT and sealed in a 25 mL flask fitted with a magnetic stirrer bar. The solution was then deoxygenated by purging thoroughly with nitrogen for 15 min, heated to 90 °C in an oil bath, and allowed to react for 24 h. The resulting solution was centrifuged for 5 min at 4000 rpm and the supernatant was precipitated into hexane and dissolved in THF three times. The precipitate was then dissolved in water and purified by dialysis, yielding a pink viscous solid after freeze drying.

2.4 Reduction of the polymer end groups to free thiol groups

Polymers with the terminal RAFT groups were reduced to the thiol by aminolysis in the presence of n-hexyl amine using a 4:1 molar ratio to the poly(OEGMA-*co*-PFPEMA) copolymer and catalytic amount of dimethylphenyl phosphine (DMPP) to prevent the formation of disulfides (1 mol %).

2.5 Conjugation of poly(OEGMA-co-PFPEMA) with N-(5-fluoresceinyl)maleimide dye

The procedure for attachment of the fluorescent dye was as follows: an aqueous solution of poly(OEGMA-*co*-PFPEMA) (100 mg, 0.005 mmol) was gradually titrated into a DMSO solution containing N-(5-fluoresceinyl)maleimide (2.3 mg, 0.0054 mmol). The pH was adjusted to ~ 6 and the mixture was allowed to react at room temperature in the dark for 24 h. A yellow product was obtained after dialysis against water and freeze drying. The wavelengths of the maxima in excitation and emission of the dye were 492 nm and 518 nm, respectively.

2.6 Cell culture of human mesenchymal stem cells

Third trimester placentas were acquired from healthy mothers with uncomplicated pregnancies at term during elective caesarean section (CS), as approved by The Human Research Ethics Committee of the Royal Brisbane and Women's Hospital. Informed consent was obtained from the

human subjects. MSCs were isolated from the maternal side of the placenta (decidua). *Decidua*-derived MSCs were cultured in Dulbecco's modified Eagle medium (DMEM, Invitrogen), supplemented with 10% fetal bovine serum (FBS), 1% antibiotic-antimycotic (AA), at 37 °C in a humidified atmosphere, with 5% CO_2. Cells were passaged at 90% confluency at a ratio of 1:2 or 1:3.[52] The PMSCs were characterized and fulfilled the minimal criteria established by the International Society of Cellular Therapy (ISCT).[53]

2.7 ^{19}F NMR analysis of cellular uptake

The extent of internalization of the polymers by PMSCs was quantified using ^{19}F NMR. Cells were grown to 90% confluency in T175 flasks, and then incubated with media containing polymer at different concentrations (1, 3, 5, 10, 15 and 20 mg mL^{-1}) for 24 hours to determine the optimal labelling concentration. The total cell number was determined using a hemocytometer with Trypan blue exclusion. An average of 2 x 10^6 cells was required per condition. Labelled cells were assayed for ^{19}F content by NMR as previously described.[10, 46] A known number of cells was placed in lysis buffer and mixed with D_2O and trifluoroacetic acid (TFA) as the ^{19}F NMR standard compound. ^{19}F NMR spectra of the cell pellets were acquired with a delay time of 10 s and 128 scans. The mean number of ^{19}F nuclei per cell (F_c) was calculated using Equation (1).

$$F_c = \frac{3.I_s.M_r.N_a}{I_r N_c} \qquad (1)$$

Where (I_s/I_r) is the ratio of the integrated intensities of the PFPE peak in the cell pellet divided by that of the trifluoroacetic acid (TFA) reference peak, N_c is the number of cells in the pellet, M_r is the number of moles of the TFA reference, N_a is Avogadro's number.

2.8 Confocal microscopy

Imaging was conducted to ascertain if the copolymers were internalized by the cells. Cells were seeded onto coverslips and 3 mg mL^{-1} of poly(OEGMA-*co*-PFPEMA) conjugated with N-(5-fluoresceinyl)maleimide was added and incubated for several hours. The cells were fixed for 15 min in 4% paraformaldehyde (PFA), before being rinsed 3×5 min in phosphate-buffered saline (PBS). Subsequently, ActinRed™ 555 reagent (ThermoFisher) which selectively labels F-actin was added

to the fixed cells and incubated for 30 minutes, before being rinsed 3×5 min in (PBS) and mounted with DAPI in Vectashield. ActinRed™ 555 dye is excited at a wavelength of 540 nm and has an emission maximum at 565 nm. Images were acquired using a Zeiss LSM 710 inverted confocal microscope and were analyzed using ZEN software (Zeiss).

2.9 Quantifying cell labelling using flow cytometry

Cells labelled with polymer were seeded at a density of 100,000 cells/well in a 24 well plate. Different concentrations (0, 1, 3, 5, 10, 15 mg mL^{-1}) of the copolymer were added to the media. After incubation for 24 hours, cells were trypsinized and suspended in (PBS) for analysis using a BD LSR II Flow Cytometer. The relative fluorescence intensity per condition was obtained.

2.10 Retention of copolymer in PMSCs

Cells were stained with Trypan Blue and counted using a haemocytometer to measure cell proliferation, at specific time points. Dilution and retention of copolymers were assessed by seeding cells at a density of 100,000 cells/well in a 24 well plate. Cells were incubated with copolymers for 24 hours and copolymer that was not internalized were washed off with PBS. Subsequently, cells were trypsinized and suspended in PBS at specific time points for analysis whereby the fluorescence intensity was measured using flow cytometry. Exocytosis of copolymer was evaluated by seeding cells at a very low density/well in a 24 well plate. Cells were incubated with copolymer for 24 hours and any copolymer that was not internalized was washed off with PBS. Fluorescence intensity of cell culture media was measured at specific time points using a plate reader. To establish if there is a transfer of the copolymer from labelled to resident cells, 2×10^4 cells labelled with the bimodal copolymer were co-cultured with 2×10^4 cells labelled with the green fluorescent Cell Tracker (10 μM for 20 minutes at 37°C). Images were acquired 1, 3 and 7 days using a Zeiss LSM 710 inverted confocal microscope and were analyzed using ZEN software (Zeiss). The number of red, green and yellow cells were counted to determine transfer of the copolymer (red) into “unlabelled” (green) cells.

2.11 Cytotoxicity and viability assay

To measure the effect of the polymer on cell viability, the Trypan Blue exclusion test (Invitrogen) was conducted immediately after labelling with varying concentrations of polymer. To quantify whether the polymer affects the mitochondrial function of the cells, CCK-8 assays were conducted on ^{19}F-labelled and control cells, as described previously.[54] The CCK-8 assay measures the amount of formazan dye that is reduced by intracellular dehydrogenase. The number of living cells is proportional to the concentration of the formazan dye. Briefly, the CCK-8 solution (10 μl) was added to cells seeded in a 96-well plate and incubated for four hours. Absorbance was read on a Tecan plate reader at a wavelength of 450 nm.

2.12 Tri-lineage differentiation assay

To assess the effect of uptake of the copolymers on tri-lineage differentiation, MSCs were grown in twelve well plates for adipogenic, osteogenic and chondrogenic assays. Three wells were incubated with the copolymers for 24 hours and another three wells were utilized for the unlabelled PMSCs (control). After 24 hours, the wells were washed with PBS and adipogenic/osteogenic/chondrogonenic media (Thermofisher StemPro^{R} differentiation kit) were added according to manufacturer's instructions. The media was replaced every 3-4 days. After 21 days, the cells were fixed with 4% PFA and stained with Alizarin Red S to detect calcification, Oil Red O for identification of lipid vesicles and Toluidine Blue for staining of the chondrogenic pellet. Images were captured on a Nikon inverted microscope equipped with a Phantom V9 high speed color camera. The images were post processed in ImageJ software.

2.13 Expression of MSC markers

To determine the potential effect of labelling with the copolymers on the phenotypical characteristics, MSCs were cultured in a flask till confluency. PMSCs were incubated with copolymers for 24 hours and flask was washed with PBS before detachment and suspended according to manufacturer's guide (BD Human MSC Analysis Kit) in staining solution. Cells were incubated with antibodies as per instructions and analyzed on a flow cytometer, Accuri C6. Flow Jo Software was used for data processing.

2.14 Standard protocol for labelling MSCs with poly(OEGMA-co-PFPEMA)

Based on the results of measurement of cellular uptake and viability, a concentration of polymer solution of 10 mg mL^{-1} and incubation time of 24 hours were determined to be optimal conditions for uptake of the polymer by human derived PMSCs. Cells were seeded into a T75 culture flask and grown to 90% confluency prior to labelling with the polymer using the conditions immediately above. PBS was added to the flask and decanted (washing step) to remove excess copolymers and Tryple Express was added to dissociate the cells from the flask. Cell suspensions with PBS were centrifuged at 400 g for 5 minutes (three times) and the cell pellet was resuspended in PBS to remove excess copolymers. Cells were resuspended for all subsequent experiments.

2.15 Preparation of cell phantoms

^{19}F MRI phantoms consisting of $0.4x10^6$, $0.8x10^6$, $1.6x10^6$, and $3.2x10^6$ cells labelled with 10 mg mL^{-1} of copolymers were suspended in a (50 μl) volume of 6% gelatin in Eppendorf tubes. A control consisting of unlabelled PMSCs in a (50 μl) volume of 6% gelatin in a tube was imaged together with the ^{19}F phantoms. Samples were loaded with increasing cell numbers in order to determine the threshold for cell detection. This procedure yields an estimate of the concentration of cells that can be detected upon transplantation given the particular hardware configuration, imaging methods employed, and the time constraints of *in vivo* imaging.[46]

2.16 ^{19}F MRI and measurement of NMR relaxation times

In vitro MRI - All MR images were acquired on a 9.4 T Bruker system using a $^1H/^{19}F$ dual resonator 40 mm volume coil. Co-localization and positioning of slices for the ^{19}F scan was achieved using an ^1H MR scan that was acquired using a rapid acquisition with relaxation enhancement (RARE) sequence (RARE factor = 16, TE = 88 ms, TR = 1500 ms, FOV = 80 × 80 mm, matrix = 128 × 128), 4 slices at 2 mm thickness. The ^{19}F images were acquired using a RARE sequence (TR = 1500 ms, TE = 44 ms, RARE factor = 8, averages = 256, FOV = 80 × 80 mm, matrix size = 64 × 64, single slice at 20 mm thickness, 51 mins scan time). $^1H/^{19}F$ images were analyzed using Image J software.

In vivo MRI - Experiments were carried out in accordance with the national guidelines provided and approved by the institutional animal care and ethics committees of the University of Queensland. Labelled human PMSCs (~ 1 x 10^6) were injected subcutaneously into the right flank of a 12-week old female non-obese diabetic/severe combined immunodeficient (NOD SCID) mouse. 24 hours post injection of labelled PMSCs, the mouse was anesthetized with an intraperitoneal (IP) injection of ketamine/xylazine in water and placed in the scanner. ^{1}H images were acquired using a RARE sequence (TR = 1500 ms, TE = 10 ms, RARE factor = 4, FOV = 58 × 58 mm, matrix = 128 × 128, 12 slices at 2 mm thickness). The ^{19}F images were acquired using a RARE sequence (TR = 1500 ms, TE = 10 ms, slice thickness = 2 mm, RARE factor = 4, Matrix = 64 x 64, in-plane resolution = 0.9 mm). ^{1}H/^{19}F images were analyzed using Osirix software.

2.17 Quantification of MRI

The intensity of the signal in a particular voxel of a ^{19}F MR image is proportional to the total number of ^{19}F nuclei within that volume. To calculate the signal-to-noise ratio (SNR) in the ^{19}F MR images, the average signal was obtained in a region of interest (ROI) consisting of 49 voxels for each phantom (0, 0.4, 0.8, 1.6, and 3.2 x 10^6 PMSCs). The SNR was determined based on Equation (2):

$$\text{SNR} = \frac{\text{Mean Signal (labelled cells) - Mean Background Signal}}{\text{Standard deviation of background}} \qquad (2)$$

The measured phantom SNR was plotted as a function of cell number. The minimum cell per voxel detection threshold was established by extrapolating the SNR to a value of 1.5 for unequivocal detection of labelled cells.

3. RESULTS AND DISCUSSION

3.1 Characterization of Poly(OEGMA-*co*-PFPEMA) Copolymer

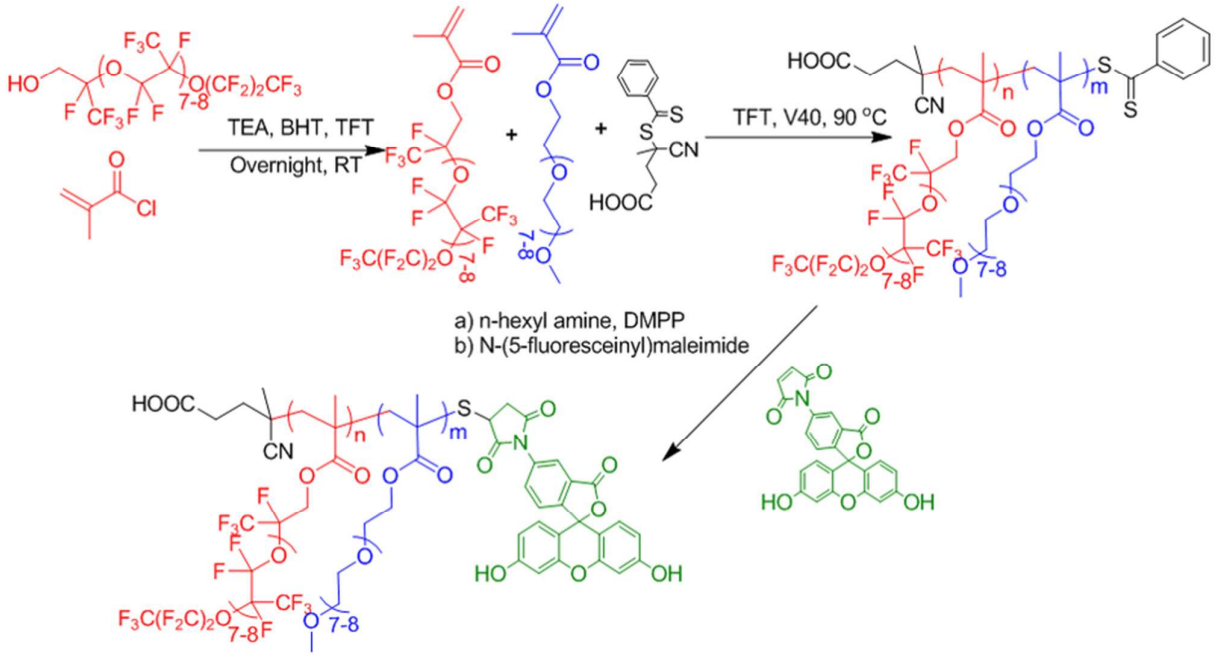

Scheme 1. Schematic diagram illustrating the synthesis of poly(OEGMA-*co*-PFPEMA) copolymers via RAFT polymerization and the labelling with green fluorescence dye Mal*N*Flu.

The synthetic approach for the preparation of functionalized PFPE-based polymers is illustrated in (Scheme 1). A polymerizable methacrylate of PFPE (PFPEMA) was first synthesized by a standard elimination reaction between methacryloyl chloride and the monohydroxy-terminated PFPE. Typical ^{1}H NMR spectra in $CDCl_3$ and the assignments to the spectra of the PFPE and PFPEMA are shown in Figure S1. The peak located at ~4.7 ppm in the NMR spectrum of PFPEMA can be assigned to the methylene protons of PFPE segments adjacent to the ester, confirming the successful attachment of the PFPE to the polymerizable methacrylate unit.

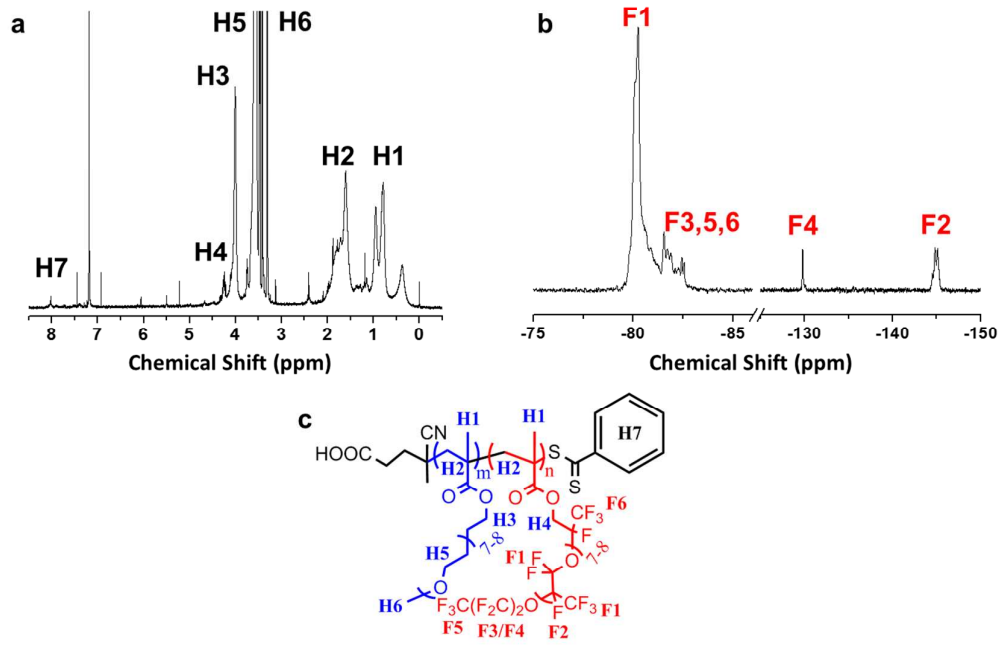

Figure 1. (a) ^{1}H and (b) ^{19}F NMR spectra in $CDCl_3$ and assignments to the spectra of the poly(OEGMA-*co*-PFPEMA). (c) The chemical structure of the poly(OEGMA-*co*-PFPEMA) showing labels for assignment of the NMR spectra.

Statistical copolymers of PFPEMA and OEGMA were synthesized through RAFT polymerization. As shown in Figure S2, the conversion of OEGMA and PFPEMA monomers to polymer during the polymerization could be determined from the integrated intensities in the ^{1}H NMR spectrum of the crude sample (85 % and 78 %, respectively). Typical ^{1}H and ^{19}F NMR spectra of the poly(OEGMA-*co*-PFPEMA) copolymer after purification and the relevant assignments are shown in Figure 1. The molecular weight and composition of the copolymer can be calculated from the integrals of the peaks arising from protons H3, H4 and the RAFT agent proton H7 as shown in Figure 1a. It can be concluded that the number-average molecular weight of the poly(OEGMA-*co*-PFPEMA) copolymer is ~75000 g mol^{-1} and the ratio of OEGMA to PFPEMA repeat units within the copolymer is approximately equal to seven. The observation of a value of $M_{n,NMR}$ larger than the theoretical value ($M_{n,th}$) may indicate the loss of RAFT end groups during polymerization. The fluorine content was calculated to be 21.4 wt %, which is significantly higher than for previously reported fluorinated polymers for MRI applications (typically below 5 wt %).[27, 30-33] The peaks in

the ^{19}F NMR spectrum (Figure 1b) were assigned successfully based on previous reports and the integrated intensities of each peak correspond to the number of fluorine atoms in the chemical structure (Figure 1c).[55, 56] It should be noted that the most intense peak, due to the fluorinated methyl and methylene groups (ca. -80 ppm, F1 in the spectrum), dominates the spectrum and will predominantly contribute to the subsequent ^{19}F MRI signal. The hydrodynamic diameter of the copolymer was approximately 12 nm as measured using DLS, indicating the molecules were present as unimers in solution. To achieve conjugation with a fluorescent dye, the RAFT end group of the copolymer was reduced to free thiol in the presence of n-hexyl amine. *N*-(5-fluoresceinyl)maleimide, a green fluorescent dye, was directly conjugated to the copolymer, creating a dual modality imaging agent. The properties of the polymers deduced from the detailed characterization are summarized in Table S1 in the Supporting Information.

The ^{19}F NMR T_1 and T_2 relaxation times of the copolymers, important for MRI applications, were measured by dissolving the polymer in PBS/D_2O (90/10, v/v) at a concentration of 20 mg mL^{-1} at 310 K. The values of ^{19}F NMR T_1 and T_2 at 9.4 T were 410 ms and 60 ms, respectively. The ^{19}F NMR T_1 and T_2 relaxation times in labelled cells, i.e. of the polymer within PMSCs, were 420 ms and 62 ms, respectively. It can be concluded from these values that the copolymer after uptake by PMSCs is suitable for MR imaging with a high signal-to-noise ratio *in vitro.* Furthermore the values of NMR T_1 and T_2 did not change after cell uptake, indicating the absence of large changes in the spectral density of high (MHz) and low (kHz) frequencies of motion of the polymer.

3.2 Efficiency of labelling of human PMSCs with poly(OEGMA-*co*-PFPEMA)

To assess the efficiency of labelling human PMSCs with poly(OEGMA-*co*-PFPEMA), the cells were incubated with cell culture media containing polymer at a range of concentrations. Cell uptake was assessed by ^{19}F NMR, and corroborated by flow cytometry and confocal microscopy.

3.2.1. ^{19}F NMR analysis to quantify fluorine content per cell

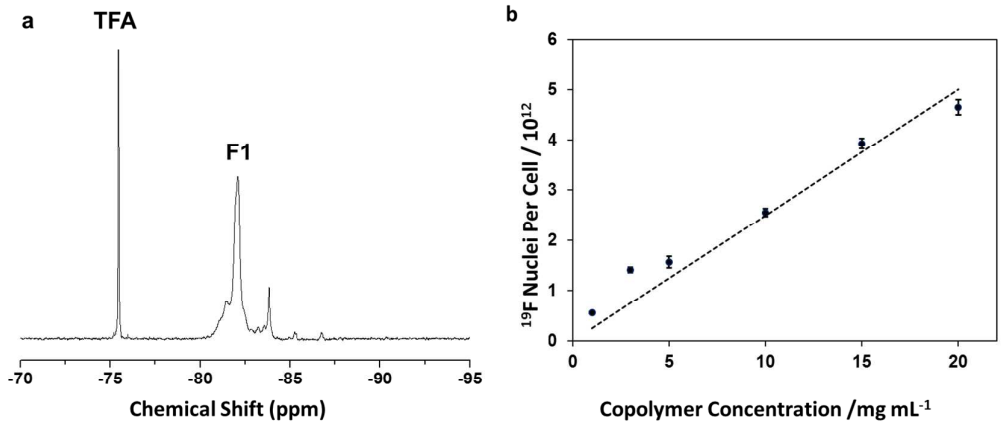

Figure 2. a) ^{19}F NMR spectrum of 2 x 10^6 cells labelled with 20 mg mL^{-1} of copolymer. Peak F1 of the copolymer, see Figure 1 b), is centered at ~82 ppm. TFA was used as a reference and gives a peak at -75.5 ppm. 2b) Plot of number of ^{19}F nuclei per cell against concentration of poly(OEGMA-*co*-PFPEMA) in the incubation medium. MSCs were incubated at different concentrations for 24 hours. All values are presented as mean ± standard deviation.

A quantitative measure of the intracellular fluorine content was obtained by comparison of the intensity in the ^{19}F NMR spectrum to that of a reference standard (trifluoroacetic acid, TFA). Well-defined peaks in the ^{19}F NMR spectra are observed at −76 ppm for TFA and major peaks between −80 to -85 ppm for the labelled cells Figure 2a. Integration of the peaks allowed the extent of cell uptake to be calculated, and this was found to increase in proportion to the concentration of the copolymer in the incubation media (Figure 2a). The content of observable fluorine nuclei (Figure 2b) is comparable or superior to results reported for MSCs[12, 21, 46, 57] and other therapeutically-relevant cells[58-60] labelled with PFPE nanoemulsions. Hence, cell uptake achieved with our copolymers, without addition of transfection agent, is within suitable limits and comparable with other published reports.

Recently, a number of researchers have studied the effects of size, shape and surface chemistry (for e.g. surface hydrophobic/hydrophilic balance, surface charge, zeta potential) on cellular uptake and toxicity of nanoparticles. In brief, smaller sized and more hydrophobic molecules are internalized and leave cells more rapidly.[61, 62] The high level of uptake of poly(OEGMA-*co*-PFPEMA) by the PMSCs, without the assistance of transfection agents or electroporation, is likely a consequence of

the small size of the copolymer (hydrodynamic diameter of ~12 nm) and partial hydrophobic nature resulting from its high fluorine content (21.4 wt %). We suggest that the conformational flexibility inherent in the polymeric structure allows the hydrophobic groups to be presented to the cell membrane, thus facilitating passage across the membrane.

The ability to load the cells without the use of transfection agents is a major advantage as transfection agents may not be suitable for clinical use. Transfection techniques can be utilized to potentially increase the uptake of agents in cells but these may adversely affect cellular functions, for instance inducing a down-regulation of surface marker expression.[43] Furthermore, comprehensive studies of the effects of transfection techniques on the function, phenotype and proliferation in different cell types have not been reported. [63] Hence, it is highly attractive that non-phagocytic cells such as MSCs are able to be labelled efficiently with MR trackers by simple co-incubation in the culture media.

3.2.2 Confocal microscopic study of cellular uptake

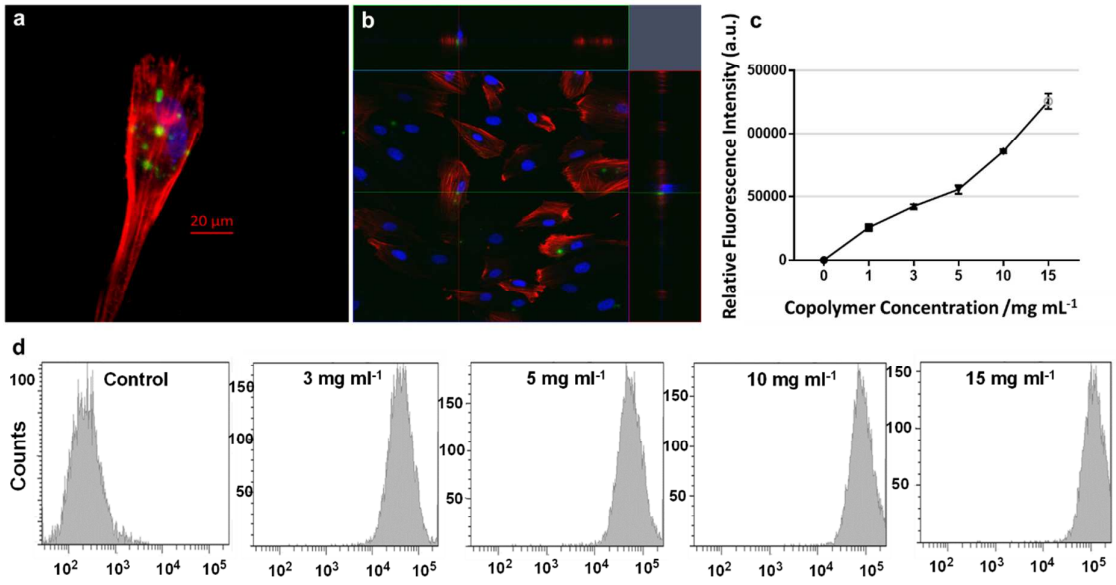

Figure 3. Confocal fluorescence images of MSCs labelled with 3 mg $mL^{-1}$of Poly(OEGMA-*co*-PFPEMA) with *N*-(5-fluoresceinyl)maleimide for 3 hours. The nuclei were stained with DAPI (blue), copolymer (green) and actin was stained red a) 40x magnification, size bar = 20 µm. b) Ortho projection of 3D image. 20x magnification. All experiments were performed at least three times and representative images are shown. Excitation wavelengths were 358 nm, 492 nm and 540 nm, respectively. Results of flow cytometry of PMSCs incubated with increasing concentrations of Poly(OEGMA-*co*-PFPEMA) with *N*-(5-fluoresceinyl)maleimide c) Relative fluorescence intensity (measure of efficiency of cell labelling) measured by flow cytometry as a function of concentration

of copolymer in solution. Output provides values for 10 000 cells for each condition. d) Fluorescence histograms.

Cell labelling studies were carried out using poly(OEGMA-*co*-PFPEMA) conjugated with *N*-(5-fluoresceinyl)maleimide dye to act as a fluorescent reporter. Figure 3a shows confocal fluorescence microscopy images of the PMSCs incubated with 3 mg mL^{-1} of poly(OEGMA-*co*-PFPEMA)-DYE for three hours. Note that the boundaries of the PMSCs were labelled with ActinRed™ 555 reagent. The ortho-projection of the 3D image indicates that the copolymers have been taken up and reside within the cells (Figure 3b & Video S1). Therefore, the confocal fluorescence images confirm internalization of the copolymers within the cytoplasm and more precisely into vesicles of the cells (Figure 3a-b). Importantly no differences in morphology between labelled and unlabelled PMSCs were observable.

3.2.3 Quantifying cell labelling using flow cytometry

Flow cytometry of PMSCs incubated with poly(OEGMA-*co*-PFPEMA) with attached *N*-(5-fluoresceinyl)maleimide in solutions of varying concentrations confirms that the extent of cell uptake is directly proportional to polymer concentration in the incubation media (Figure 3c and d). These results are in line with measurements of fluorine content by ^{19}F NMR (Figure 2b).

3.3 Proliferation of PMSCs and Cytotoxicity of copolymers

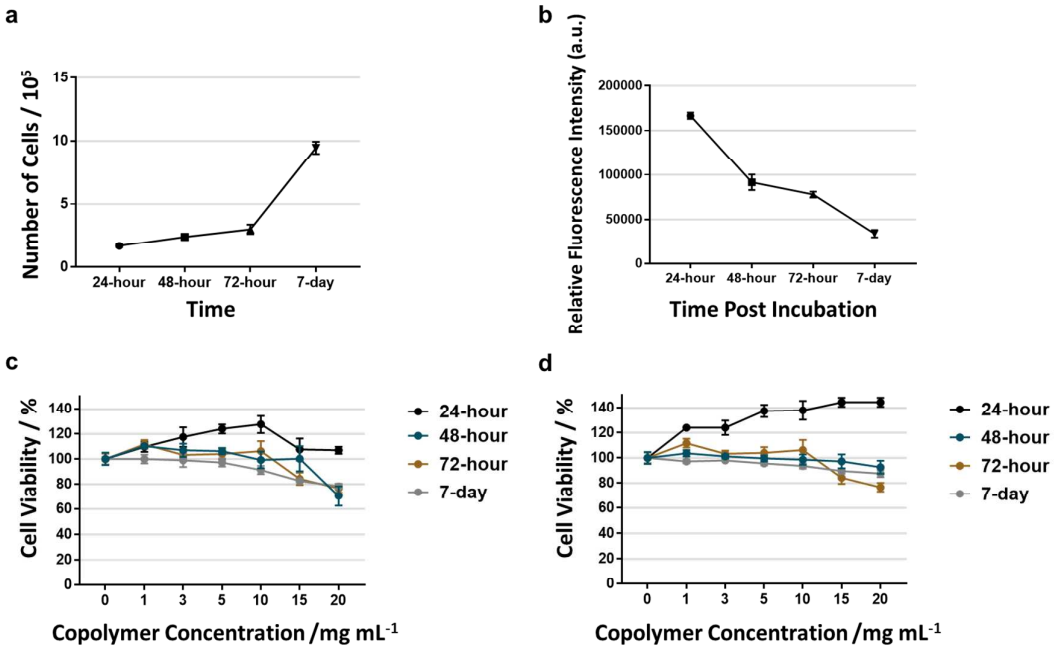

Figure 4. a) Proliferation of PMSCs at specific time points. b) Relative fluorescence intensity (measure of fluorescence dilution of copolymers) measured by flow cytometry as a function of time after incubation with the copolymers in solution. The output provides values for 10 000 cells for each condition. c) and d) Viability of PMSCs evaluated by CCK-assay and MTS assay as a function of concentration of poly(OEGMA-*co*-PFPEMA) solution. All values are presented as mean ± standard deviation based on triplicated samples.

Proliferation of the PMSCs resulted in dilution of the copolymers and a steady reduction in the amount of copolymer present in the cells (Figure 4a-b). Nonetheless, a significant fluorescence signal was observed even after 7 days of cell proliferation. This decline in copolymers signal intensity was also observed in our longitudinal *in vivo* ^{19}F MR imaging studies. This decrease is most likely due to the dilution of copolymers resulting from proliferation of cells or cell death. Cell division and consequent dilution of intracellular trackers are a challenge for long-term *in vivo* cell tracking, irrespective of the type of cell tracker.[11] Cell death can result in dispersion of tracer and loss of MRI detectability. In addition, it is possible that some copolymer chains will be exocytosed from the MSCs and internalized by bystander cells such as resident macrophages. This may produce false positive signals if a large number of these macrophages accumulates in an area of interest.[43]

Successful translation of materials to clinical applications depends on favorable cytocompatibility. Hence, CCK-8 assays were performed on PMSCs incubated with solutions of copolymers from 24 hours to 7 days post incubation to examine cytotoxicity and proliferation of the cells. The results in Figure 4c indicate that there was a slight increase (~13%) in viability and mitochondrial activity of PMSCs exposed to solutions of poly(OEGMA-*co*-PFPEMA) at 20 mg mL^{-1} for 24 hours. Nonetheless, cell viability was more than 80% at all time-points and concentrations except at the highest concentration of 20 mg mL^{-1}, 7 days after copolymer exposure (~78% cell viability). Viability of the cells was also confirmed by the MTS assay (Figure 4d) and the Trypan blue exclusion assay (Figure S3). The assays indicate that the copolymers did not have a significant effect on the viability and mitochondrial function of the PMSCs. Based on the measurements of labelling efficiency and viability, a protocol of labelling of PMSCs with 10 mg mL^{-1} of poly(OEGMA-*co*-PFPEMA) for 24 hours was adopted as the standard procedure.

3.4 Effects of copolymer uptake on typical PMSC characteristics

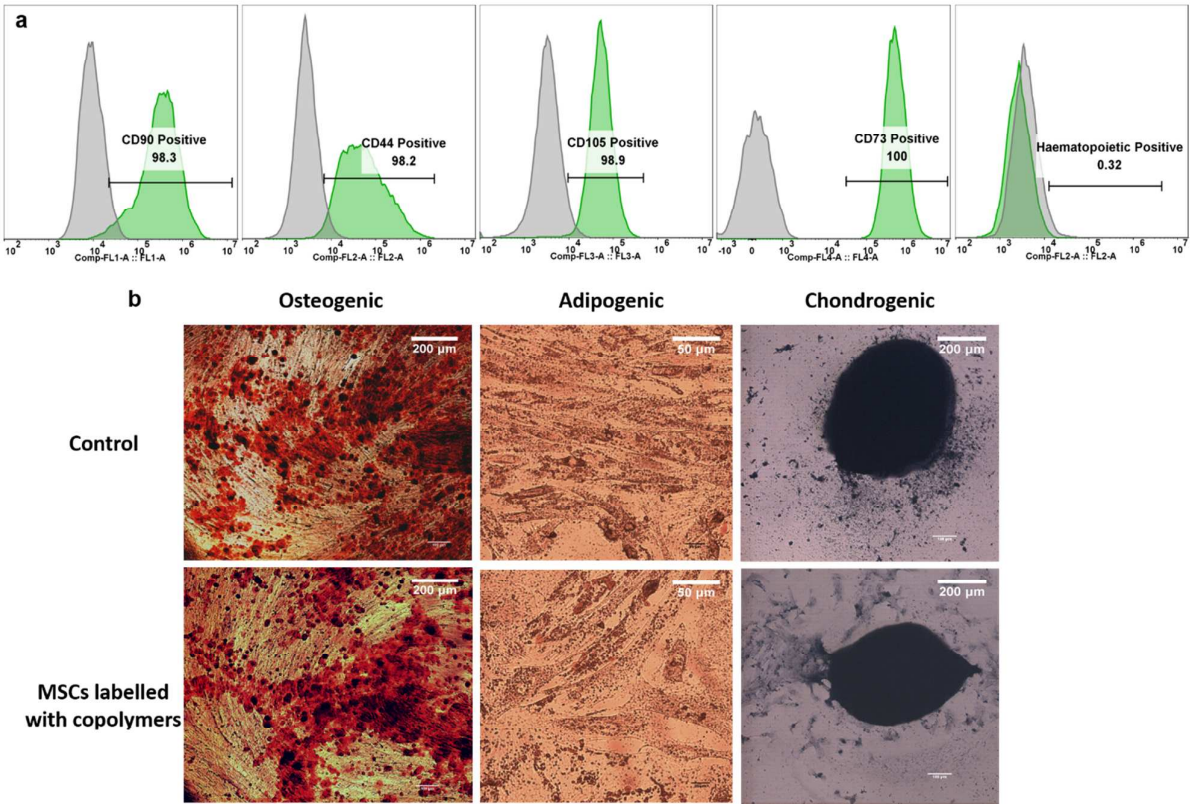

Figure 5. a) Expression of MSC markers (CD44, CD73, CD90 and CD105) and lack of specific markers (CD34, CD11b, CD45 and HLA-DR) in PMSCs after labelling with copolymers b) Bright

field microscopy images of osteogenic, adipogenic and chondrogenic differentiation of PMSCs after labelling with copolymers (bottom panel), PMSCs with no copolymers (upper panel). Scale bars: 200 μm (adipogenic and chondrogenic) 50 μm (adipogenic). No differences between labelled and unlabelled cells were observed for tri-lineage differentiation. All experiments were performed at least three times and representative images are shown.

It is important that MRI cell trackers do not affect the phenotype, differentiation potential and function of the MSCs as any alterations after labelling could impact upon the efficacy of the MSC therapy. Therefore, the PMSCs labelled with copolymers were comprehensively assessed according to the criteria established for MSCs by the International Society for Cellular Therapy (ISCT) for i) plastic adherence ii) expression of specific MSCs markers and lack of HSC markers, and iii) tri-lineage differentiation potential. The results presented in Figure 5a demonstrate that more than 98% of cell populations expressed MSC markers (CD44, CD73, CD90 and CD105) with negligible (0.32%) expression of HSC markers (CD11b, CD19, CD34, CD45 and HLA-DR). Additionally, after 21 days of treatment with osteogenic differentiation medium, osteoblasts were observed by staining with Alizarin Red which binds to calcium matrix deposits (Figure 5b bottom left panel). PMSCs labelled with the copolymers were also able to differentiate into adipocytes, demonstrated by the presence of lipid droplets (Figure 5b bottom panel). Additionally, labelled MSCs displayed chondrogenic capability, exhibited by the toluidine blue stained chondrogenic pellet (Figure 5b bottom right panel). Finally, MSCs labelled with the copolymers maintained plastic adherence under standard cell culture conditions.

3.5 Establishing a threshold for cell detection by ^{19}F MRI

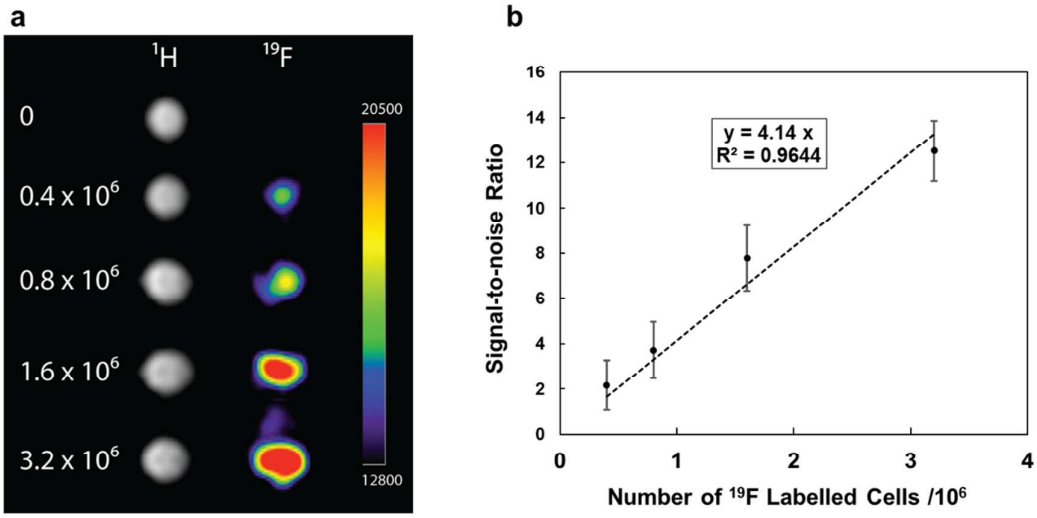

Figure 6. a) ^{1}H and ^{19}F MRI of phantoms containing 0 = Unlabelled control, 0.4 x 10^6, 0.8 x 10^6, 1.6 x 10^6 and 3.2 x 10^6 labelled pMSCs suspended in 6% gelatin. Images are shown using different colourimetric scales to allow clear visualization. b) ^{19}F MRI SNR plotted against the number of cells labelled with copolymer. Error bars are over n=3 technical replicates.

For any MRI application it is important to establish the detection limit for labelled cells. To achieve this, ^{19}F MRI scans of a set of phantoms were prepared containing 0.4 x 10^6 to 3.2 x 10^6 PMSCs labelled with 10 mg mL^{-1} of poly(OEGMA-*co*-PFPEMA) by incubation for 24 hours, and ^{19}F MRI images were acquired. This allowed determination of the signal threshold for cell detection. T_2-weighted images were acquired, using a scan time of 50 minutes, for both labelled and control unlabelled cells (2 x 10^6 cells). Signals from all phantoms containing cells were readily detected in this time period, and significantly the phantom with the smallest number of cells (0.4 x 10^6) also had a detectable ^{19}F MRI signal (Figure 6a). As anticipated, the ^{19}F MR signal intensity (and hence signal-to-noise ratio, SNR) increased linearly with the number of cells (Figure 6b). If we propose a target SNR of 1.5 to permit unequivocal detection of labelled cells, we find that a minimum of 3.6×10^5 cells labelled with copolymer in this manner is required for cell detection. Considering the cell pellet and voxel size, this results in a detection limit of $\sim 7.4 \times 10^3$ *cells/voxel*. To put this into perspective, a typical MSC based clinical therapy requires multiple intravenous infusion of cell numbers in the range of millions.[64, 65] It is very clear therefore that the cell detection limit of less

than 10^4 cells/voxel attained with PMSCs labelled with poly(OEGMA-*co*-PFPEMA) is within the required range for tracking of stem cells. Previous studies involving tracking of PFPE labelled cells using MRI have reported minimum cell detection sensitivity in the order of 10^4 to 10^5 cells/voxel with clinical MRI scanners and 10^3 to 10^4 for high field animal scanners. Therefore, the cell detection limit achieved here with PMSCs labelled with these unique copolymers is comparable to data reported with high field animal scanners.[14, 43, 45, 66] We conclude that MSCs labelled with these copolymers have potential to enhance efficacy of stem cell therapies by informing on suitable injection sites, and confirming routes of migration and accumulation cell numbers at the engraftment site.

3.6 Retention of the Copolymers in PMSCs

Proliferation of the PMSCs resulted in a steady reduction in the amount of copolymers present in the cells (Figure 7a-c). Nonetheless, a significant fluorescence signal was observed via flow cytometry even after 7 days following incubation with the copolymer (Figure 7b, black bars). The confocal microscopy z-stack images (Figure S4 & S5) also confirm retention of the copolymers until the endpoint of the experiment. A decrease in signal intensity was also observed in our *in vivo* ^{19}F MR longitudinal imaging studies, and is most likely due to the dilution of the copolymers resulting from proliferation of cells or cell death. Cell division and consequent dilution of intracellular trackers are a challenge in long term *in vivo* cell tracking, for all approaches to cell tracking.[11] In addition, cell death can result in dispersion of tracer and loss of detectable MRI signal.

Exocytosis (leakage) of copolymers can also contribute to the reduction in fluorescence intensity, and was assessed by measuring the fluorescence of the cell culture media at specific time points using a microplate reader. Fluorescence of the cell culture media increased gradually over time,

indicating that a small portion of the copolymers was released across this period (Figure 7b, red bars). The cells were confirmed to be viable (Trypan blue exclusion, data not shown) and therefore the fluorescence in the media does not arise from copolymers released by dead cells. Nonetheless, the intensity of fluorescence arising from exocytosis is relatively low in comparison to the significant fluorescence retained within the MSCs (Figure 7b). It is also possible that copolymers may be exocytosed by cells and internalized by bystander cells such as resident macrophages. This may produce false positive signals if a large number of macrophages accumulates in an area of interest.[43] To assess this probability, cells labelled with copolymer (red fluorescence) were co-cultured with cells labelled green (Cell Tracker, Figure 7c). DAPI-positive cells with both red and green signals were observed as yellow via confocal imaging. At day one post co-culture, approximately 25% of the cells were yellow indicating that some exocytosis and transfer of copolymers to neighboring cells had occurred. As pointed out by Bible et al.,[46] some of this fluorescence may arise from dead cells or from residual unwashed copolymer. Those authors observed similar levels of label transfer in cells labelled with Celsense. After three and seven days of co-culture, 27% and 21% of the DAPI positive cells were yellow, respectively, demonstrating that exocytosis and transfer of the copolymer to the bystander cells remains constant up to seven days after *in vitro* labelling. It is clear that the potential for transfer of label to bystander cells needs to be critically evaluated for clinical applications. However, the observation that the level of label transfer remains close to constant up to seven days means that this level of transfer can be subtracted from observed levels to allow *in vivo* quantification of labelled SMCs after topical injection. In addition, the observed level of label transfer is only clinically significant if a large number of these cells accumulates in the region of interest. In line with this, the majority of animal studies of injected cells labelled with SPIOs have demonstrated negligible transfer from labelled cells to macrophages.[18, 67-70] Hence, we contend that concern about phagocytic engulfment of labelled cells should not hamper future research in this field.

As anticipated, the number of cells retaining copolymers (red cells) visualized by confocal microscopy decreased by approximately half at day seven. This decrease is predominantly due to dilution of the copolymers on proliferation of the cells. In conclusion, despite the ready uptake of the copolymers by the PMSCs, leakage of copolymer is minimal and there is sufficient retention to allow excellent *in vivo* imaging.

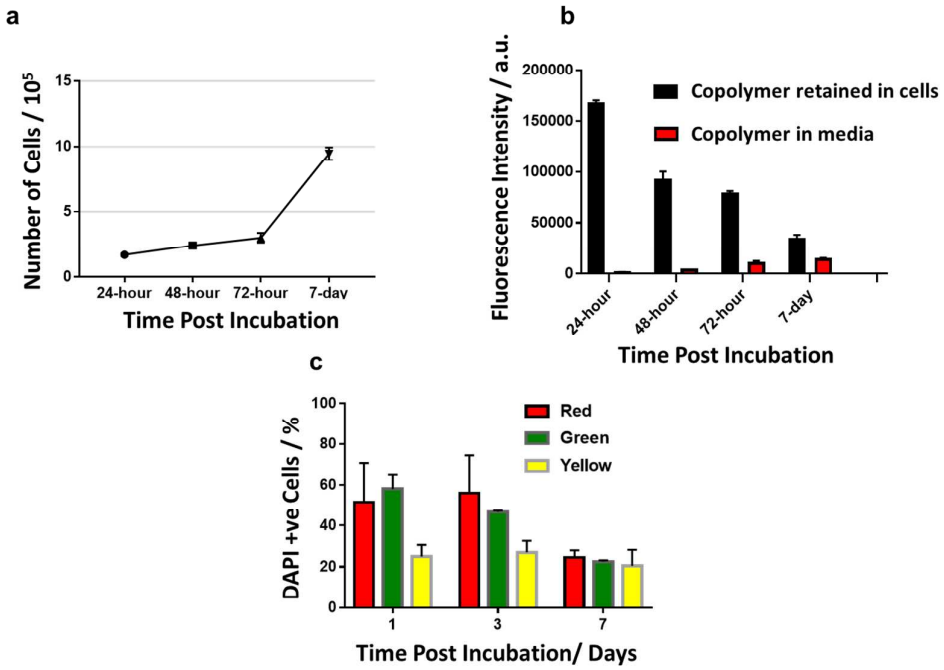

Figure 7. a) Proliferation of PMSCs at specific time points b) Fluorescence intensity (measure of retention of copolymers in PMSCs) measured by flow cytometry as a function of time after incubation with copolymers (black bars). The fluorescence is for 10,000 cells at each time point. The fluorescence intensity of cell culture media due to exocytosed copolymer (red bars). c) Co-culturing of cells labelled either with the bimodal copolymers (red fluorescence) and with bystander cells (labelled with green cell tracker). All values are the mean ± standard deviation based on measurements in triplicate.

3.7 Tracking of cell fate with *in vivo* ^{19}F MRI

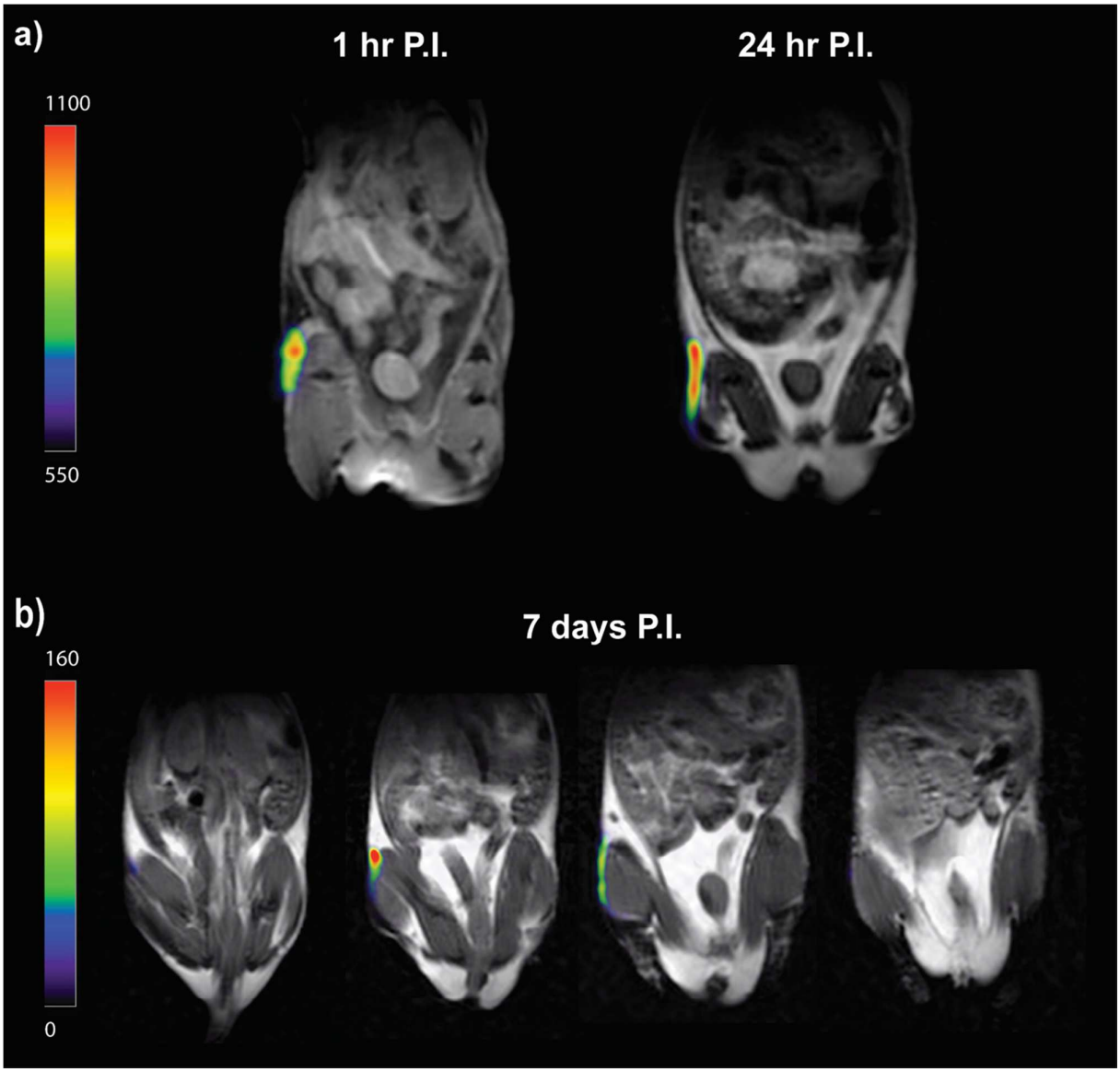

Figure 8. *In vivo* detection of labelled human PMSCs injected subcutaneously in a NOD-SCID mouse. Images shown are 1, 24 hours and 7 days post injection and anatomical overlay of $^{19}F/^{1}H$ images, whereby the ^{19}F is rendered in false color and ^{1}H is in grayscale. MSCs are visible as a "hot spot" in the flank of mouse. a) Images acquired from 1 and 24 hours post injection, 51 minutes scan. Slice thickness = 20 mm b) Images acquired from 7 days post injection, 12 minutes scan. Slice thickness = 2 mm. The arrow denotes slices containing ^{19}F signal.

The feasibility of detecting cells *in vivo* has been demonstrated by subcutaneous injection of cells into a murine model. ^{19}F MRI was performed at 1 hour, 24 hours and 7 days post injection of ~ 1 x 10^6 labelled human PMSCs into the right subcutaneous flank of a NOD SCID mouse. Strong and unequivocal signals from labelled cells were clearly detected in ^{19}F MR images acquired at 9.4 T, 1 hour and 24 hours post injection (Figure 8a). Moreover, distinct signals from labelled cells at the

site of injection were observed 7 days post injection within a short acquisition time of 12 minutes (Figure 8b). However, we noted a slight reduction in ^{19}F MR signal intensity between days 1 and 7 post injection of the labelled MSCs. Previously Bible *et al.* used ^{19}F MRI to measure neural stem cells (NSCs) labelled with Celsense and suspended in a bioscaffold implanted into the lesion cavity of a rat stroke model. As in the current study, they observed a decrease in ^{19}F MRI signal between days 1 and 7 post implantation.[46] Our results with labelled MSCs are therefore in accordance with other longitudinal imaging studies which established a decrease in signal from the tracker over time.[21, 44, 45] The decline in ^{19}F MR signal is expected and is probably due to cell proliferation or cell death which results in dilution of the copolymers as demonstrated in the *in vitro* studies (Figure 4a-b). Importantly, the animals did not appear to suffer deleterious effects throughout the experiments. The mice were observed twice daily throughout the 7 days following injection of the labelled cells. The mice appeared healthy and did not exhibit any characteristic signs and symptoms of illness. Note that to strictly avoid false positive ^{19}F MR signals from gaseous anesthesia such as isoflurane, IP injection of ketamine/xylazine was utilized for anesthesia for *in vivo* imaging.

4. CONCLUSIONS

In summary, we have reported the successful synthesis of a unique partially-fluorinated polymer as a dual MR/fluorescence imaging agent. The copolymer with a hydrodynamic diameter of 12 nm has a high fluorine content of >20 %, substantially higher than previously reported partially-fluorinated polymers (< 5 wt. %) intended for MRI applications. Furthermore, the polymer can be functionalized in a facile manner, as demonstrated by the development of a dual-mode fluorescence-MRI imaging agent by conjugation of a dye molecule to the copolymer. Our results demonstrate that PMSCs can be efficiently labelled with these new fluorinated copolymers, without the use of transfection agents, and with negligible deleterious effects on the viability, mitochondrial and phenotypic function of the cells. Additionally, we were able to measure ^{19}F MR images of labelled cell phantoms, and show that the imaging performance is equal or superior to previously developed materials. Preliminary *in vivo* ^{19}F MRI data showed that labelled PMSCs could be

readily detected up to seven days post injection within a short MRI acquisition scan period (12 minutes). We conclude that the copolymers reported here show outstanding potential to be utilized as imaging agents for ^{19}F MRI-based tracking and quantification of non-phagocytic and therapeutically-relevant cells such as MSCs.

ASSOCIATED CONTENT

Supporting Information. Electronic Supplementary Information (ESI) available: NMR spectroscopy, details of characteristics of copolymers, confocal z-stack images and viability assay.

AUTHOR INFORMATION

Corresponding Author

*E-mail: a.whittaker@uq.edu.au

‡ These authors contribute equally to this work.

Conflicts of interest

There are no conflicts to declare.

Acknowledgements

The authors acknowledge the Australian Research Council (CE140100036, DP0987407, DP110104299, LE0775684, LE0668517, and LE0882357) and the National Health and Medical Research Council (APP1021759) for funding of this research. The Australian National Fabrication Facility, Queensland Node, is also acknowledged for access to some items of equipment. We thank Dr Rebecca Pelekanos and Ms Varda Sardesai from UQCCR for their assistance in isolation and characterization of MSCs, Joyce Tang for her aid in characterization of labelled MSCs and Dr Nyoman Kurniawan for assistance with the MRI measurements.

REFERENCES

1. S. M. Millard and N. M. Fisk, *BioEssays*, 2013, **35**, 173-182.
2. Y. Wang, C. Xu and H. Ow, *Theranostics*, 2013, **3**, 544-560.
3. S. Wang, X. Qu and R. Zhao, *Journal of Hematology & Oncology*, 2012, **5**, 19.
4. P.-M. Chen, M.-L. Yen, K.-J. Liu, H.-K. Sytwu and B.-L. Yen, *Journal of Biomedical Science*, 2011, **18**, 49.
5. K. Shah, *Biomatter*, 2013, **3**.
6. L. Y. Chien, J. K. Hsiao, S. C. Hsu, M. Yao, C. W. Lu, H. M. Liu, Y. C. Chen, C. S. Yang and D. M. Huang, *Biomaterials*, 2011, **32**, 3275-3284.
7. M. Srinivas, E. H. J. G. Aarntzen, J. W. M. Bulte, W. J. Oyen, A. Heerschap, I. J. M. de Vries and C. G. Figdor, *Advanced Drug Delivery Reviews*, 2010, **62**, 1080-1093.
8. A. Rosenzweig *New England Journal of Medicine*, 2006, **355**, 1274-1277.
9. M. S. Thu, J. Najbauer, S. E. Kendall, I. Harutyunyan, N. Sangalang, M. Gutova, M. Z. Metz, E. Garcia, R. T. Frank, S. U. Kim, R. A. Moats and K. S. Aboody, *PLoS One*, 2009, **4**, e7218.
10. J. M. Janjic and E. T. Ahrens, *Wiley interdisciplinary reviews. Nanomedicine and nanobiotechnology*, 2009, **1**, 492-501.
11. E. T. Ahrens and J. W. Bulte, *Nat Rev Immunol*, 2013, **13**, 755-763.
12. P. Boehm-Sturm, L. Mengler, S. Wecker, M. Hoehn and T. Kallur, *PLoS One*, 2011, **6**, e29040.
13. M. Srinivas, A. Heerschap, E. T. Ahrens, C. G. Figdor and I. J. de Vries, *Trends Biotechnol*, 2010, **28**, 363-370.
14. E. T. Ahrens, R. Flores, H. Xu and P. A. Morel, *Nat Biotech*, 2005, **23**, 983-987.
15. R. Weissleder, G. Elizondo, J. Wittenberg, C. A. Rabito, H. H. Bengele and L. Josephson, *Radiology*, 1990, **175**, 489-493.
16. J. V. Frangioni and R. J. Hajjar, *Circulation*, 2004, **110**, 3378-3383.
17. E. Bull, S. Y. Madani, R. Sheth, A. Seifalian, M. Green and A. M. Seifalian, *International Journal of Nanomedicine*, 2014, **9**, 1641-1653.
18. C. Chapon, J. Jackson, E. Aboagye, A. Herlihy, W. Jones and K. Bhakoo, *Molecular Imaging and Biology*, 2009, **11**, 31-38.
19. C. Heyn, J. A. Ronald, L. T. Mackenzie, I. C. MacDonald, A. F. Chambers, B. K. Rutt and P. J. Foster, *Magnetic Resonance in Medicine*, 2006, **55**, 23-29.
20. U. Himmelreich, R. Weber, P. Ramos-Cabrer, S. Wegener, K. Kandal, E. M. Shapiro, A. P. Koretsky and M. Hoehn, *Molecular imaging*, 2005, **4**, 104-109.
21. E. J. Ribot, J. M. Gaudet, Y. Chen, K. M. Gilbert and P. J. Foster, *Int J Nanomedicine*, 2014, **9**, 1731-1739.
22. S. C. Berman, C. Galpoththawela, A. A. Gilad, J. W. M. Bulte and P. Walczak, *Magnetic resonance in medicine : official journal of the Society of Magnetic Resonance in Medicine / Society of Magnetic Resonance in Medicine*, 2011, **65**, 564-574.
23. J. Ruiz-Cabello, B. P. Barnett, P. A. Bottomley and J. W. M. Bulte, *NMR in Biomedicine*, 2011, **24**, 114-129.
24. I. Tirotta, V. Dichiarante, C. Pigliacelli, G. Cavallo, G. Terraneo, F. B. Bombelli, P. Metrangolo and G. Resnati, *Chemical Reviews*, 2015, **115**, 1106-1129.

25. M. Srinivas, P. Boehm-Sturm, C. G. Figdor, I. J. de Vries and M. Hoehn, *Biomaterials*, 2012, **33**, 8830-8840.
26. H. Peng, I. Blakey, B. Dargaville, F. Rasoul, S. Rose and A. K. Whittaker, *Biomacromolecules*, 2009, **10**, 374-381.
27. K. J. Thurecht, I. Blakey, H. Peng, O. Squires, S. Hsu, C. Alexander and A. K. Whittaker, *Journal of the American Chemical Society*, 2010, **132**, 5336-5337.
28. K. Wang, H. Peng, K. J. Thurecht, S. Puttick and A. K. Whittaker, *Polym. Chem.*, 2014, **5**, 1760-1771.
29. K. Wang, H. Peng, K. J. Thurecht, S. Puttick and A. K. Whittaker, *Polym. Chem.*, 2013, **4**, 4480-4489.
30. B. E. Rolfe, I. Blakey, O. Squires, H. Peng, N. R. B. Boase, C. Alexander, P. G. Parsons, G. M. Boyle, A. K. Whittaker and K. J. Thurecht, *Journal of the American Chemical Society*, 2014, **136**, 2413-2419.
31. C. Zhang, S. S. Moonshi, H. Peng, S. Puttick, J. Reid, S. Bernardi, D. J. Searles and A. K. Whittaker, *ACS Sensors*, 2016, **1**, 757-765.
32. C. Zhang, H. Peng and A. K. Whittaker, *Journal of Polymer Science Part A: Polymer Chemistry*, 2014, **52**, 2375-2385.
33. C. Zhang, H. Peng, S. Puttick, J. Reid, S. Bernardi, D. J. Searles and A. K. Whittaker, *Macromolecules*, 2015, **48**, 3310-3317.
34. K. Wang, H. Peng, K. J. Thurecht, S. Puttick and A. K. Whittaker, *Biomacromolecules*, 2015, **16**, 2827-2839.
35. K. Wang, H. Peng, K. J. Thurecht, S. Puttick and A. K. Whittaker, *Polym. Chem.*, 2016, **7**, 1059-1069.
36. H. Peng, K. J. Thurecht, I. Blakey, E. Taran and A. K. Whittaker, *Macromolecules*, 2012, **45**, 8681-8690.
37. K. Wang, H. Peng, K. J. Thurecht and A. K. Whittaker, *Macromol. Chem. Phys.*, 2016, **217**, 2262-2274.
38. C. Zhang, S. S. Moonshi, Y. Han, S. Puttick, H. Peng, B. J. A. Magoling, J. C. Reid, S. Bernardi, D. J. Searles, P. Král and A. K. Whittaker, *Macromolecules*, 2017, **50**, 5953-5963.
39. C. Fu, S. Herbst, C. Zhang and A. K. Whittaker, *Polym. Chem.*, 2017, **8**, 4585-4595.
40. E. Önal, C. Zhang, D. Davarcı, Ü. İşci, G. Pilet, A. K. Whittaker and F. Dumoulin, *Tetrahedron Lett.*, 2017, DOI: 10.1016/j.tetlet.2017.12.032.
41. W. Zhao, H. T. Ta, C. Zhang and A. K. Whittaker, *Biomacromolecules*, 2017, **18**, 1145-1156.
42. G. E. Gerhardt and R. J. Lagow, *The Journal of Organic Chemistry*, 1978, **43**, 4505-4509.
43. M. Srinivas, P. A. Morel, L. A. Ernst, D. H. Laidlaw and E. T. Ahrens, *Magnetic Resonance in Medicine*, 2007, **58**, 725-734.
44. P. Boehm-Sturm, M. Aswendt, A. Minassian, S. Michalk, L. Mengler, J. Adamczak, L. Mezzanotte, C. Löwik and M. Hoehn, *Biomaterials*, 2014, **35**, 2218-2226.
45. J. Ruiz-Cabello, P. Walczak, D. A. Kedziorek, V. P. Chacko, A. H. Schmieder, S. A. Wickline, G. M. Lanza and J. W. Bulte, *Magn Reson Med*, 2008, **60**, 1506-1511.
46. E. Bible, F. Dell'Acqua, B. Solanky, A. Balducci, P. M. Crapo, S. F. Badylak, E. T. Ahrens and M. Modo, *Biomaterials*, 2012, **33**, 2858-2871.
47. P. Taylor, *Advances in Colloid and Interface Science*, 1998, **75**, 107-163.
48. K. J. Thurecht, *Macromolecular Chemistry and Physics*, 2012, **213**, 2567-2572.
49. C. Pipino, P. Shangaris, E. Resca, S. Zia, J. Deprest, N. J. Sebire, A. L. David, P. V. Guillot and P. De Coppi, *British Medical Bulletin*, 2012, DOI: 10.1093/bmb/lds033.
50. P. S. in 't Anker, S. A. Scherjon, C. Kleijburg-van der Keur, G. M. J. S. de Groot-Swings, F. H. J. Claas, W. E. Fibbe and H. H. H. Kanhai, *Stem cells (Dayton, Ohio)*, 2004, **22**, 1338-1345.
51. Y. Mitsukami, M. S. Donovan, A. B. Lowe and C. L. McCormick, *Macromolecules*, 2001, **34**, 2248-2256.

52. N. Matigian, G. Brooke, F. Zaibak, T. Rossetti, K. Kollar, R. Pelekanos, C. Heazlewood, A. Mackay-Sim, C. A. Wells and K. Atkinson, *Genomics Data*, 2015, **3**, 70-74.
53. R. A. Pelekanos, V. S. Sardesai, K. Futrega, W. B. Lott, M. Kuhn and M. R. Doran, *J. Visualized Exp.*, 2016, **6**, 54204.
54. A. Blocki, S. Beyer, J.-Y. Dewavrin, A. Goralczyk, Y. Wang, P. Peh, M. Ng, S. S. Moonshi, S. Vuddagiri, M. Raghunath, E. C. Martinez and K. K. Bhakoo, *Biomaterials*, 2015, **53**, 12-24.
55. T. E. Karis, B. Marchon, D. A. Hopper and R. L. Siemens, *J. Fluorine Chem.*, 2002, **118**, 81-94.
56. Z. Zhang, X. Hao, P. A. Gurr, A. Blencowe, T. C. Hughes and G. G. Qiao, *Aust. J. Chem.*, 2012, **65**, 1186-1190.
57. J. M. Gaudet, E. J. Ribot, Y. Chen, K. M. Gilbert and P. J. Foster, *PLoS ONE*, 2015, **10**, e0118544.
58. M. Srinivas, M. S. Turner, J. M. Janjic, P. A. Morel, D. H. Laidlaw and E. T. Ahrens, *Magn. Reson. Med.*, 2009, **62**, 747-753.
59. E. T. Ahrens, B. M. Helfer, C. F. O'Hanlon and C. Schirda, *Magn. Reson. Med.*, 2014, **72**, 1696-1701.
60. B. M. Helfer, A. Balducci, A. D. Nelson, J. M. Janjic, R. R. Gil, P. Kalinski, I. J. M. de Vries, E. T. Ahrens and R. B. Mailliard, *Cytotherapy*, 2010, **12**, 238-250.
61. G. Oenbrink, P. Jurgenlimke and D. Gabel, *Photochem. Photobiol.*, 1988, **48**, 451-456.
62. S. Kang, S. H. Bhang, S. Hwang, J.-K. Yoon, J. Song, H.-K. Jang, S. Kim and B.-S. Kim, *ACS Nano*, 2015, **9**, 9678-9690.
63. M. Carlsten and R. Childs, *Front. Immunol.*, 2015, **6**, 266.
64. D. C. Chambers, D. Enever, N. Ilic, L. Sparks, K. Whitelaw, J. Ayres, S. T. Yerkovich, D. Khalil, K. M. Atkinson and P. M. A. Hopkins, *Respirology*, 2014, **19**, 1013-1018.
65. F. D. Lublin, J. D. Bowen, J. Huddlestone, M. Kremenchutzky, A. Carpenter, J. R. Corboy, M. S. Freedman, L. Krupp, C. Paulo, R. J. Hariri and S. A. Fischkoff, *Mult. Scler. Relat. Disord.*, 2014, **3**, 696-704.
66. K. C. Partlow, J. Chen, J. A. Brant, A. M. Neubauer, T. E. Meyerrose, M. H. Creer, J. A. Nolta, S. D. Caruthers, G. M. Lanza and S. A. Wickline, *FASEB J*, 2007, **21**, 1647-1654.
67. J. W. Bulte, L. Kostura, A. Mackay, P. V. Karmarkar, I. Izbudak, E. Atalar, D. Fritzges, E. R. Rodriguez, R. G. Young, M. Marcelino, M. F. Pittenger and D. L. Kraitchman, *Academic radiology*, 2005, **12 Suppl 1**, S2-6.
68. D. L. Kraitchman, A. W. Heldman, E. Atalar, L. C. Amado, B. J. Martin, M. F. Pittenger, J. M. Hare and J. W. M. Bulte, *Circulation*, 2003, **107**, 2290-2293.
69. J. J. Graham, W. D. Foltz, A. K. Vaags, M. R. Ward, Y. Yang, K. A. Connelly, R. Vijayaraghavan, J. S. Detsky, M. R. Hough, D. J. Stewart, G. A. Wright and A. J. Dick, *American Journal of Physiology-Heart and Circulatory Physiology*, 2010, **299**, H125-H133.
70. D. J. Stuckey, C. A. Carr, E. Martin-Rendon, D. J. Tyler, C. Willmott, P. J. Cassidy, S. J. Hale, J. E. Schneider, L. Tatton, S. E. Harding, G. K. Radda, S. Watt and K. Clarke, *Stem cells (Dayton, Ohio)*, 2006, **24**, 1968-1975.

For table of contents only

A Unique ^{19}F MRI Agent for the Tracking of Non Phagocytic Cells *In Vivo.*

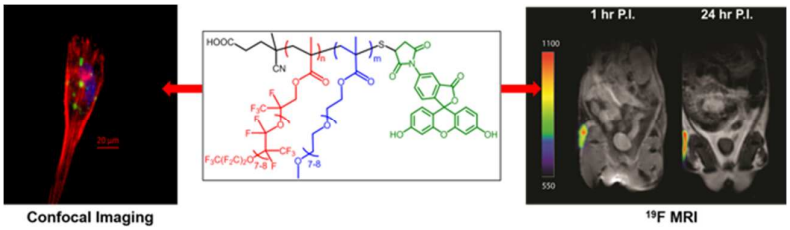

We describe the synthesis and characterization of a novel PFPE-based partially fluorinated copolymer for *in vivo* tracking of MSCs.